Biomaterials Science

ROYAL SOCIETY OF CHEMISTRY

PAPER

View Article Online
View Journal

Published on 26 April 2021. Downloaded by University of Prince Edward Island on 5/16/2021 7:57:57 AM.

Check for updates

Cite this: DOI: 10.1039/d0bm01825b

In vivo micro computed tomography detection and decrease in amyloid load by using multifunctionalized gold nanorods: a neurotheranostic platform for Alzheimer's disease†

Francisco Morales-Zavala,[a,b,c] Pedro Jara-Guajardo,[a,b] David Chamorro,[d,e] Ana L. Riveros,[a,b] America Chandia-Cristi,[d,e] Nicole Salgado,[f] Paola Pismante,[g] Ernest Giralt,[h,i] Macarena Sánchez-Navarro,[h] Eyleen Araya,[b,j] Rodrigo Vasquez,[a,j] Gerardo Acosta,[k] Fernando Albericio,[k,l] Alejandra Alvarez R *[d,e] and Marcelo J. Kogan *[a,b]

Received 26th October 2020,
Accepted 11th April 2021

DOI: 10.1039/d0bm01825b

rsc.li/biomaterials-science

The development and use of nanosystems is an emerging strategy for the diagnosis and treatment of a broad number of diseases, such as Alzheimer's disease (AD). Here, we developed a neurotheranostic nanosystem based on gold nanorods (GNRs) that works as a therapeutic peptide delivery system and can be detected *in vivo* for microcomputed tomography (micro-CT), being a diagnostic tool. GNRs functionalized with the peptides Ang2 (a shuttle to the Central Nervous System) and D1 (that binds to the Aβ peptide, also inhibiting its aggregation) allowed detecting differences *in vivo* between wild type and AD mice (APPswe/PSEN1dE9) 15 minutes after a single dose by micro-CT. Moreover, after a recurrent treatment for one month with GNRs-D1/Ang2, we observed a diminution of amyloid load and inflammatory markers in the brain. Thus, this new designed nanosystem exhibits promising properties for neurotheranostics of AD.

[a]*Departamento de Química Farmacológica y Toxicológica, Facultad de Ciencias Químicas y Farmacéuticas, Universidad de Chile, Santiago, Chile. E-mail: mkogan@ciq.uchile.cl*
[b]*Advanced Center for Chronic Diseases (ACCDiS), Sergio Livingstone 1007, Independencia, Santiago, Chile*
[c]*Centro de Nanotecnología Aplicada, Facultad de Ciencias, Universidad Mayor, Camino La Piramide 5750, Huechuraba, Chile*
[d]*Facultad de Ciencias Biológicas, Pontificia Universidad Católica de Chile, Alameda 340, Santiago 8331010, Chile. E-mail: aalvarez@bio.puc.cl*
[e]*Centro de envejecimiento y regeneración (CARE), Facultad de Ciencias Biológicas, Pontificia Universidad Católica de Chile, Santiago, Chile*
[f]*Unidad de Microscopía Avanzada, Facultad de Ciencias Biológicas, Pontificia Universidad Católica de Chile, Santiago, Chile*
[g]*Departamento de Tecnologías Nucleares, División de Investigación y Aplicaciones Nucleares, Comisión Chilena de Energía Nuclear, Chile*
[h]*Institute for Research in Biomedicine (IRB Barcelona), Barcelona Institute of Science and Technology (BIST), Baldiri Reixac 10, Barcelona, 08028, Spain*
[i]*Department of Inorganic and Organic Chemistry, University of Barcelona, Martí I Franqués 1-11, Barcelona, 08028, Spain*
[j]*Departamento de Ciencias Quimicas, Facultad de Ciencias Exactas, Universidad Andres Bello, Santiago, Chile*
[k]*CIBER-BBN, Networking Centre on Bioengineering, Biomaterials and Nanomedicine & Department of Organic Chemistry, Marti i Franques 1-11, University of Barcelona (UB), 08028 Barcelona, Spain*
[l]*School of Chemistry & Physics, University of KwaZulu-Natal, Durban 4001, South Africa*

†Electronic supplementary information (ESI) available. See DOI: 10.1039/d0bm01825b

1. Introduction

Multifunctional nanomaterials have aroused growing interest in the medicinal field, especially for the diagnosis and treatment of several diseases and as drug delivery systems. In particular, multifunctionalized gold nanoparticles (GNPs) can be utilized for bioimaging and in phototherapy, integrating them into one system with both diagnostic and therapeutic functions, and therefore being considered for "theranostics".[1]

The most remarkable property of GNPs is that they exhibit a localized surface plasmon (LSP), which allows GNRs to absorb light in the so-called biological window, and their ability to produce heat also makes it possible to use them for photothermal therapy.[2–4] Additionally, GNPs are already used at the preclinical level, as a contrast agent for computed tomography (CT) due to their high X-ray attenuation.[5–7] Bio-imaging has been explored as a diagnostic tool for neurodegenerative disorders for several years using different techniques, such as magnetic resonance imaging (MRI), positron emission tomography (PET) or single-photon emission computed tomography (SPECT).[8,9] However, PET and SPECT are expensive and require the availability of a synchrotron for the preparation of radioactive probes, which makes them of difficult access for diagnosis in large parts of the population.

Published on 26 April 2021. Downloaded by University of Prince Edward Island on 5/16/2021 7:57:57 AM.

In contrast, CT is an inexpensive technique, and its main limitation is related to the selectivity for the detection between soft tissues. This limitation can be overcome by the selective targeting of contrast agents to the target tissue, increasing the ability to discriminate different kinds of the anomalous structures in soft tissues. In this context, and due to their X-ray attenuation properties, GNPs are the best contrast imaging agents for CT.[5,6,10] Moreover, GNPs are highly susceptible to functionalization, which allows efficient active targeting – a key feature that is very relevant for an efficient drug delivery system.[11–13] Indeed, GNPs targeted to myocardial scars have been used for scar size evaluation by CT in rats[10] and GNP-labeled exosomes have been detected by CT in the central nervous system of mice; therefore, CT and GNPs constitute an economical, fast and noninvasive system to perform diagnosis *in vivo*.[6] Furthermore, GNPs exhibit excellent compatibility with humans, low toxicity, and stability. Recent studies have revealed that GNPs can cross the blood–brain barrier (BBB).[12] Importantly, clinical trials with GNPs are currently in progress, with promising results for cancer, arthritis and cardiovascular diseases.[14–21]

Alzheimer's disease (AD) is the most common cause of dementia among older adults. Although AD pathological hallmarks and molecular mechanisms are known, early diagnosis and the development of effective therapies remain as main scientific challenges. With this in mind, our research group has explored the use of GNPs as a strategy for designing new theranostic options for AD.[4,11,12,22]

The accumulation of β-amyloid (Aβ) peptide in the brain is an important and reliable pathological biomarker of AD, but it is believed that it also triggers the synaptic dysfunction and neurodegeneration that underlie cognitive decline in AD patients.[23,24] The pathological Aβ toxic aggregates (oligomers, fibers, and amyloid plaques) produce oxidative stress and neurotoxicity.[25–27] In previous publications we have evaluated the AD diagnostic and therapeutic potential of GNPs (different shapes; rods and spheres), functionalized with peptides designed to inhibit Aβ aggregation.[3,28,29] Recently, we used gold nanorods (GNRs) functionalized with two peptides: peptide D1, which recognizes and disaggregates amyloid aggregates, and Angiopep-2 (Ang2, with sequence TFFYGGSRGKRNNFKTEEY), which favors crossing the BBB, to disaggregate Aβ and reduce the toxicity of the aggregates *in vivo*. The D1 peptide has the ability to inhibit Aβ peptide aggregation and promote Aβ aggregate disaggregation. D1 (which has the H-qshyrhispaqv-OH sequence) is formed by D amino acids that are stable against endogenous proteases.[30–32] We have previously demonstrated the *in vivo* effect of GNRs functionalized with D1 and with Ang2 (GNRs-D1/Ang2) by the administration of this nanosystem in a *Caenorhabditis elegans* AD model (CL2120 strain), where we observed inhibition of the Aβ aggregation process and a diminution of its toxic effects.[11]

In this work, in a further and key step, we evaluated another *in vivo* approach, using a murine model of AD, to test the capacity of the nanosystem to be delivered to the brain, the effects on the amyloid load and inflammation in the brain,

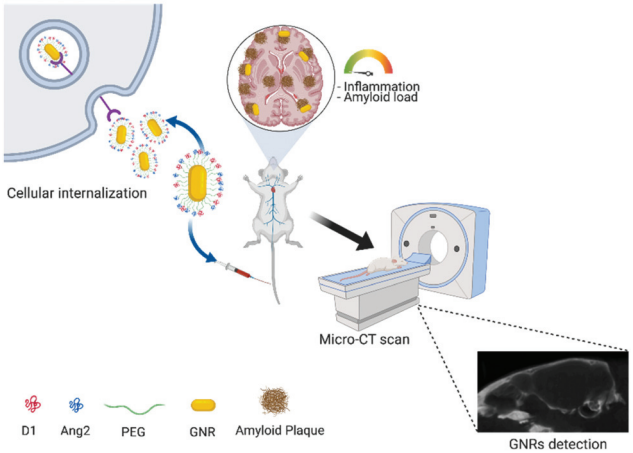

Scheme 1 Evaluation of cell penetration (*in vitro*), brain delivery (*in vivo*), amyloid plaque attachment (*ex vivo*) and *in vivo* detection by micro-CT of GNRs-D1/Ang2.

and the potential use of GNRs-D1/Ang2 as a detection device through the CT methodology (Scheme 1). The use of GNPs as a contrast agent for CT imaging has been explored at the preclinical level for cancer, cardiovascular disease and brain stroke diagnostics, among others.[6,10,33] Nonetheless, to the best of our knowledge, the methodology of GNRs targeted against Aβ aggregates has not been explored yet for the detection of Aβ aggregates in the CNS, and is reported here for the first time, constituting a great challenge.

2. Materials and methods

2.1 GNRs synthesis

GNRs were synthesized using the growth seed-mediated approach.[3,34] In the first step, a seed solution was prepared to reduce 250 μL of $HAuCl_4$ (Sigma Chemical Co., St Louis, MO, USA) in 9.75 mL of cetyltrimethylammonium bromide 0.1 M (CTAB) (Sigma Chemical Co., St Louis, MO, USA) and cold-prepared sodium borohydride (600 μL, 0.01 M) (Sigma Chemical Co., St Louis, MO, USA). Seeds were kept at 27 °C for two hours before use. Next, 55 μL of ascorbic acid 0.1 M (Sigma Chemical Co., St Louis, MO, USA) was added to a growth solution containing 75 μL of $AgNO_3$ 0.01 M (Sigma Chemical Co., St Louis, MO, USA), 9.5 mL of CTAB 0.1 M and 500 μL of $HAuCl_4$ 0.01 M. Then, 250 μL of HCl 0.1 M and finally 12 μL of the previously prepared seed solution were added. The solution was incubated for 10 minutes at 27 °C before centrifugation at 5900*g* for 15 min. After centrifugation, the supernatant was removed, and the pellet was resuspended in Milli-Q water. Vis-NIR absorption spectra were recorded at room temperature using a PerkinElmer Lambda 25 spectrophotometer. GNRs-CTAB were observed using a scanning electron microscope with an electronic transmission module (STEM) FEI Inspect F50. The specimens for electron microscopy observation were prepared by dropping GNRs on Formvar carbon-

 This journal is © The Royal Society of Chemistry 2021

Published on 26 April 2021. Downloaded by University of Prince Edward Island on 5/16/2021 7:57:57 AM.

coated copper microgrids (Ted Pella, Inc. Redding, CA, USA) and letting them dry. The Ang2 and D1 peptides were synthetized and characterized as described by Velasco-Aguirre *et al.*[12] and Jara-Guajardo *et al.*[22]

2.2 GNRs PEGylation and peptide conjugation

PEGylation was performed as described in Huang *et al.*, 2010.[35] Briefly, peptide ligands (Ang2 and D1) were conjugated to GNRs in a three-step procedure: (1) 50 μL of mPEG-SH 1 mM (MW 5 K, JenKem Technology, TX, USA) was added to 10 mL of GNRs 1 nM, and the solution mixture was stirred for 10 min. PEGylated GNRs (GNRs-PEG) were centrifuged at 20 800*g* for 10 min and were resuspended in 10 mL Milli-Q water. (2) 300 μL of HOOC-PEG-SH 1 mM (MW 5 K, JenKem Technology, Texas, USA) was added, and the solution was stirred for 1 h. The solution was centrifuged twice at 20 800*g* for 10 min and was resuspended in 100 μL of MES buffer pH 5.5. (3) 0.2 mg EDC and 0.5 mg sulfo-NHS (Sigma Chemical Co., St Louis, MO, USA) were incubated with the functionalized GNRs for 15 min to activate the carboxyl groups on the GNRs. Excess EDC/sulfo-NHS was removed by centrifugation at 20 800*g* for 10 min, and the activated GNRs-PEG were mixed with the D1 and Ang2 peptides ligands in PBS buffer (pH 7.4) in a 1 : 1000 NR : ligand molar ratio. The solution was gently shaken for 2 h at room temperature (RT) and then stored at 4 °C. Before use, the GNRs-D1/Ang2 were washed by centrifugation to eliminate the free reactants.

We used mPEG-SH (MW 5000) because it allows to efficiently stabilize nanoparticles, avoiding their aggregation.[36] As reported, reducing the interaction with serum significantly decreases the absorption with serum protein and the interaction with macrophages, which leads to prolonged blood circulation time, as demonstrated previously by our group and others.[12,37,38]

2.3 Quantification of GNRs

A solution of GNRs was lyophilized, and the gold concentration (CAu) was determined by neutron activation analysis at the Chilean Nuclear Energy Commission (CCHEN) (see ESI†).

2.4 Quantification of peptide molecules per GNR-D1/Ang2

The number of peptide molecules per GNR-D1/Ang2 was estimated by amino acid analysis and neutron activation analysis. Once the concentration of GNRs by neutron activation analysis was obtained, we determined the number of peptide molecules that were bound to the GNRs. A GNRs-peptides solution was lyophilized and hydrolyzed for 72 h in 6 N HCl with a known quantity of aminobutyric acid as an internal standard. Afterwards, the solution was evaporated under reduced pressure and derivatized for amino acid analysis by HPLC.[11] The number of peptide molecules per GNR was calculated by dividing the number of peptide molecules per mL of solution by the number of particles per mL of solution. This ratio was calculated in triplicate from three independent analyses.

2.5 Determination of the zeta potential (pZ) quantification of GNRs

The measurements of nanoparticle zeta potential (Zeta sizer 3000, Malvern Instruments, UK) were performed by determining the electrophoretic mobility in an aqueous solution and a moderate electrolyte concentration, and calculating this potential using the Smolochowski approximation. The electrophoretic mobility measurement consisted of five repeats for each GNRs solution.

2.6 Binding of Alexa Fluor 647 to functionalized GNRs

When required, the multifunctionalized GNRs (GNRs-PEGs, GNRs-D1, GNRs-Ang2, and GNRs-D1/Ang2) were labeled with the fluorescent probe Alexa Fluor 647. Then, 500 μL of functionalized GNRs (20 nM) were washed with Milli-Q water 3 times by centrifugation (20 800*g* for 10 minutes) to remove excess free peptide remaining from the conjugation process. Then, the GNRs were resuspended in 100 μL of Milli-Q water and 10 μL of Alexa Fluor 647 (ThermoFisher) 1 mg mL^{-1} activated with a hydrazide. This group reacts in aqueous solution with carboxylic acids, aldehydes and ketones. The solution, protected from light, was incubated overnight with mechanical stirring at room temperature and then stored at 4 °C. Before use, the excess Alexa Fluor 647 was eliminated by centrifugation. The incorporation of Alexa Fluor 647 fluorescent probe on modified GNRs was evaluated using the emission spectrum at 647 nm for the functionalized GNRs (Fig. S4, ESI†).

2.7 Evaluation of cell penetration of multifunctionalized GNRs in the bEnd.3 cell line by flow cytometry

The immortalized bEnd.3 cell line from Mus musculus was used for these experiments. Cells were seeded in a 24-well plates at a density of 40 000 cells per well and after 24 hours of culture, they formed a confluent monolayer. The cells were then incubated with GNRs-PEGs, GNRs-D1 and GNRs-D1/Ang2, all Alexa Fluor 647-labeled, at a concentration of 0.05 nM for 2 hours at 37 °C (or 4 °C) (n = 5). The concentration of the nanoparticles was similar to that used in previous studies.[11,39–42] Thereafter, the cells were washed 3 times, trypsinized and harvested. Cells were washed once again, and flow cytometry analysis was performed using a Beckman Coulter CyAn ADP kit equipped with 3 lasers: 488, 643 and 405 nm. A total of 10 000 cells per sample were evaluated, and all assays were done in triplicate. For the treatment with chlorpromazine (CPZ), the cells were pretreated with CPZ for 15 minutes at a concentration of 50 μM before incubation with the GNRs (n = 6).

2.8 Evaluation of GNRs-D1/Ang2 internalization in bEnd.3 cells by TEM

The bEnd.3 cells, at a 70% confluence, were incubated with the GNR samples (GNRs-D1/Ang2, 0.05 nM). After 24 hours, the cells were washed with fresh medium and fixed with 2.5% glutaraldehyde in 0.1 M phosphate buffer. Cells were scraped from the surface, collected in an Eppendorf tube and then allowed to set overnight at 4 °C. Then, the pellet was postfixed

Published on 26 April 2021. Downloaded by University of Prince Edward Island on 5/16/2021 7:57:57 AM.

with 1% OsO_4 in phosphate buffer for 90 minutes, dehydrated in solutions with acetone gradient and finally embedded in Epon. Sections of 80 nm thickness were cut, placed over copper grids covered with carbon, and subsequently stained with uranyl acetate. Subsequently, micrographs were obtained by TEM (JEOL JEM-1010 microscope).

2.9 Evaluation of GNRs-D1/Ang2 in brains of AD mouse models by Au quantification

An AD transgenic mouse model (APPswe/PSEN1dE9, The Jackson Laboratory) was used, which corresponds to a double transgenic that expresses a mouse/human chimera of amyloid precursor protein with the Swedish mutation (Mo/HuAPP695swe) and the mutant human presenilin 1 with the Exon 9 deletion (PS1-dE9), both directed to neurons of the central nervous system (CNS). Both mutations are associated with familial AD. Mice that were 18 months of age were anesthetized intraperitoneally with ketamine xylazine (40 mg kg^{-1} and 15 mg kg^{-1}, respectively). Then, they were injected intravenously with 100 μL of a 10 nM suspension of GNRs-D1/Ang2 or GNRs-PEG. The injected doses (approximately 0.01 mg of gold per 30 g) were similar to those reported in other biodistribution studies.[43,44] At 15 minutes post-injection, the animals were perfused with PBS, and the organs of interest were obtained, frozen in liquid nitrogen and lyophilized at −50 °C under a pressure of 0.137 mbar. Once lyophilized, the dry organs were ground in a porcelain crucible to homogenize the samples. Once ground, they were placed in an oven at 120 °C until reaching a constant weight. Finally, their gold content was quantified. The experiments were performed four times in independent experiments.

2.10 Evaluation of GNRs-D1/Ang2 in brains of the AD mouse model by fluorescence

To evaluate the targeting of GNRs-D1/Ang2 into the CNS, the nanosystem was labeled with Alexa Fluor 647, and the Alexa Fluor 647-GNRs-D1/Ang2 were administered to AD transgenic mice (n = 2). As control, Alexa Fluor 647-GNRs-PEGs were administered (n = 1). The treatment was as described in the previous section. After finishing treatment, the brains were fixed by immersion in a 4% paraformaldehyde solution in PBS for 24 hours at room temperature. Once fixed, the brains were kept in a solution of 30% sucrose and stored at 4 °C until use. Using a cryostat, we obtained brain slices (30 μm). The selected slices were permeabilized with 0.4% TBS-Triton X-100, and then blocked with 0.15 M glycine for 15 minutes, 3 times with $NaBH_4$ (10 mg mL^{-1}) for 10 minutes, 50 mM ammonium chloride for 10 minutes and finally, with PBS 1×-Triton 0.2%–BSA 5% for 1 hour. The slices were incubated for 24 hours with the WO2 antibody (1 : 200 dilution in blocking solution), which selectively labels the amyloid plaques. The tissues were then washed 4 times for 10 minutes each with PBS and incubated with the secondary antibody, mouse anti-IgG conjugated to Alexa Fluor 488 (1 : 2000 in blocking solution), for 1 hour at room temperature.

Finally, images were obtained using a Carl Zeiss Microscope model Axio Imager A1, equipped with a Carl Zeiss color CCD camera model AxioCam MRc5. For fluorescence microscopy, a Mercury Lamp (Zeiss HBO 100) was used with the following sets of filters (green: Zeiss filter set 09, excitation: 450–490, emission: LP 515 and red: Zeiss filter set 45, excitation: 560/40, emission: 630/75). Carl Zeiss software AxioVision version 4.8 was used for the acquisition of images. An exposure time of 400 ms was used for the green channel and 1000 ms for the red channel.

Prior to quantifying the obtained images, contrast adjustments and background subtractions were applied using ImageJ-FIJI software to improve automated segmentation. Segmentation and data collection were performed using CellProfiler v.2.0, according to the following steps: image segmentation for both GNRs-D1/Ang2 associated labels and amyloid plaque markers, measurement of correlation between both images, evaluation of the relationship between segmented labels, classification of objects as overlapped or non-overlapped according to the relation of the specific label to amyloid plaques, masking of labels to calculate the region of GNRs-D1/Ang2 specific labelling that overlapped with amyloid, measurement of the area occupied by the overlapped region and calculation of the overlap between labels as a percentage of the total amyloid plaque area. For each treated brain, at least 6 slices were obtained independently for each analysis.

2.11 Detection of GNRs-D1/Ang2 in APPswe/PSEN1dE9 mouse brain by STEM

To confirm the presence of GNRs in the AD mice brains, we used scanning transmission electronic microscopy (STEM). The animals treated with GNRs-D1/Ang2 were perfused with PBS as described in the previous section and then perfused with a solution of 2% paraformaldehyde with 2.5% glutaraldehyde in 0.1 M sodium phosphate buffer. The brains were then extracted, and the samples were processed and observed by dark-field scanning transmission electron microscopy. See ESI† for details of the procedures.

2.12 AD mice treatment with GNRs-D1/Ang2

We used 12 month old APPswe/PSEN1dE9 mice that had free access to food and water and were maintained on a 12 h dark/light cycle in a room with controlled temperature (25 ± 2 °C). The mice were divided into five groups: free D1 peptide (n = 2), GNRs-PEG (n = 1), GNRs-D1 (n = 2), GNRs-Ang2 (n = 4), and GNRs-D1/Ang2 (n = 4). Mice received intraperitoneal (i.p.) injections of 10 nM GNRs or free D1 peptide in approximately 100 μL every two days for 30 days. The body weight of animals and their behaviors were carefully recorded daily during the extension of the experiment. One day after the last injection, mice were sacrificed, and the brains were immediately collected.

2.13 *In vivo* evaluation of multifunctionalized GNRs in the AD mouse brain by micro-CT analysis

To evaluate the scope of the multifunctionalized GNRs as a contrast agent for micro-CT, at the end of the different admin-

 This journal is © The Royal Society of Chemistry 2021

Published on 26 April 2021. Downloaded by University of Prince Edward Island on 5/16/2021 7:57:57 AM.

istrations or treatments with GNRs, the animals were scanned using a micro-CT. The animals were kept under sedation during the scanning procedure using isoflurane.

In vivo scans of the brains were performed using a micro-CT scanner (Bruker, Skyscan model 1278) with a nominal resolution of 51 μm, without aluminum filter, and with a tube voltage of 39 kV. The reconstruction was done using the SkyScanNRecon software accelerated by GPU. Ring artifact reduction, Gaussian smoothing (2%), and beam hardening correction (23%) were applied. Volume rendered 3D images were generated using the CT-Voxel ("CT-Vox") software. The experiments were carried out with $n = 3$ for the chronic treatment and $n = 1$ for the acute treatment.

2.14 Evaluation of amyloid load and inflammation in AD mice treated with GNRs-D1/Ang2

The brains obtained from the experimental groups mentioned in section 2.12 were fixed and the brain slices were manipulated as mentioned in the following sections.

2.14.1 Immunolabeling. Wild-type and APPswe/PSEN1ΔE9 mice were sacrificed, the brains were removed and fixed, and the samples were prepared as described in the previous section (section 2.1). Immunolabeling was performed with GFAP (1 : 500, Cell Signaling). Anti-mouse-Alexa Fluor-488 and anti-rabbit-Alexa Fluor 555 (1 : 1000, Molecular Probes) were used as secondary antibodies.[45]

2.14.2 Th-S staining protocol. Th-S staining was performed as previously described.[46] Briefly, brain slices of APPswe/PSEN1ΔE9 mice were dehydrated and rehydrated with ethanol and xylol batteries; then, the slices were incubated in distilled water for 10 min. Slices then were immersed in the Th-S solution (0.1% Th-S in 70% ethanol) for 5 min and washed twice in 70% ethanol for 30 s and 3 times in distilled water for 2 min. Following these washes, the sections were mounted on gelatin-coated slides and coverslipped with Dako mounting medium in the dark.[46]

2.15 Statistical analyses

The data obtained from the incorporation of GNR into the bEnd.3 cells were analyzed using Turkey's multiple comparisons statistical test. On the other hand, the data corresponding to the quantification of gold, superposition of GNR with the amyloid plaques, amyloid load, and intensity of GFAP, were analyzed using the Mann–Whitney statistical test included in the Graphpad prism 6 software.

3. Results and discussion

3.1 Characterization of GNRs-D1/Ang2

The GNRs-D1/Ang2 synthesized herein have been broadly characterized. Thus, DLS characterization showed that the GNRs had a transversal hydrodynamic diameter near 4 nm and a longitudinal hydrodynamic diameter near 68 nm (ESI†). The GNRs showed a zeta potential of −11 mV and a rod shape nanostructure, with an aspect ratio (length/width) of approximately 4 (ESI†). In the UV-VIS-NIR spectra of GNRs-D1/Ang2, we observed the presence of two characteristic peaks of absorption at 520 nm and 760 nm for the transversal and longitudinal plasmons, respectively (ESI†). The number of peptides per nanoparticle was determined by amino acid analysis and corresponded to 423 ± 23 molecules of D1 and 173 ± 36 molecules of Ang2. The information corresponding to the characterization of the control nanosystems used in this work is detailed in Table S1 and Fig. S1.† These results are in agreement with our previous work.[11]

3.2 GNRs-D1/Ang2 brain endothelial uptake

We evaluated cell penetration of GNRs-D1/Ang2 in a monolayer of bEnd.3 cells from mouse cerebral endothelium, considering that this is the first step to cross the BBB. These cells were incubated with the GNRs-D1/Ang2-Alexa647 [0.05 nM] for 2 hours, using GNRs-D1-Alexa647 as a control. Three experimental conditions were evaluated: (i) cells at 37 °C for basal endocytosis, (ii) cells at 4 °C to inhibit the energy-dependent process, and (iii) cells pretreated with chlorpromazine (CPZ), an inhibitor of clathrin-dependent endocytosis.[47] After these treatments, the cells were harvested and resuspended; the positive cellular association between Alexa-labeled GNRs and the cells was assessed by flow cytometry (Fig. 1). In the basal endocytosis condition with the GNRs-D1-Alexa Fluor647 treatment, 25% of the bEnd.3 cells were positive for fluorescence at 647 nm, while 45% of cells were positive when treated with GNRs functionalized with D1 and Ang2, similar to the result described by Velasco-Aguirre *et al.*, 2017 for the incorporation of GNRs-Ang2 in the same cell line.[12]

The Ang2 peptide has been described to cross the BBB by endocytosis *via* recognition of the LRP1 receptor, which induces clathrin-dependent endocytosis, followed by transcyto-

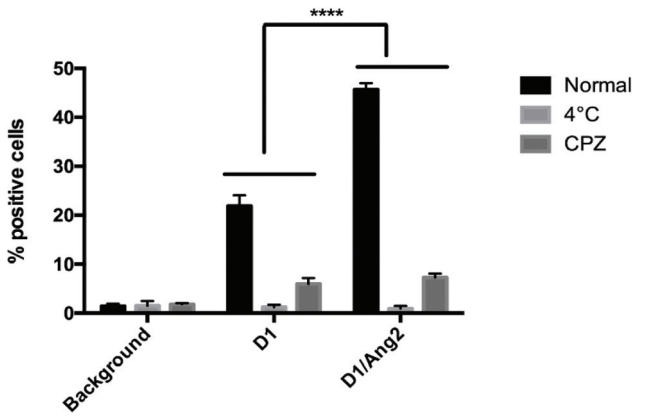

Fig. 1 Cell population positive for the incorporation of GNRs-D1 and GNRs-D1/Ang2, evaluated by flow cytometry. bEnd.3 cells were incubated for 2 hours with the different modified GNRs at a concentration of 0.05 nM. The GNRs were tagged with Alexa 647 for detection. One group of cells was incubated at 4 °C for two hours with GNRs ($n = 5$), and another group was pretreated with CPZ for 15 minutes at a concentration of 50 μM ($n = 6$). Turkey's multiple comparisons test (**** $p < 0.0001$).

Published on 26 April 2021. Downloaded by University of Prince Edward Island on 5/16/2021 7:57:57 AM.

sis.[48] We evaluated if this is the route of nanoparticle entry to the cells. As shown in Fig. 1, when both GNRs-D1 and GNRs-D1/Ang2 labelled with Alexa647 nanoparticles were incubated with bEnd.3 cells at a low temperature (4 °C) to inhibit energy-dependent processes, they did not enter to the cells. The percentage of the Alexa647-positive population observed at 2 hours of incubation decreased to levels comparable to the background, confirming that the cellular incorporation of these nanosystems is an active, energy-dependent process. Additionally, we observed a considerable decrease in the percentage of positive cells in comparison to the normal condition; in the case of GNRs-D1/Ang2, an 84% of inhibition was observed when cells were preincubated with CPZ, supporting the hypothesis that the GNRs-D1/Ang2 incorporation is clathrin-dependent. To corroborate cell internalization, we performed TEM for bEnd.3 cells incubated with GNRs-D1/Ang2 at 0.05 nM for 24 hours. The GNRs were observed inside the cells, mostly within multivesicular bodies, as shown in Fig. 2. Our results are in accordance with an incorporation of the GNRs containing the Ang2 peptide through clathrin-dependent endocytosis, probably mediated by recognition of the LRP1 receptor. The internalization was strongly inhibited by CPZ, which affects the subcellular distribution of components that form the clathrin complex.[47] This result is concordant with the TEM images, where GNRs-D1/Ang2 were observed mainly within multivesicular bodies; LRP1-mediated endocytosis in late stages of internalization directs its ligands to multivesicular bodies.[49] To evaluate the ability of GNRs-Ang2 and GNRs-D1/Ang2 to translocate across the BBB, we used an *in vitro* human BBB cellular model. Hence, human brain capillary endothelial cells from pluripotent stem cells were grown on semi-permeable membranes of a transwell, while co-cultured with bovine pericytes.[50] This BBB model resembles several of the properties of the human BBB, and has been used to study the transport of various BBB-shuttles modified with AuNP.[50–53] GNRs-Ang2 and GNRs-D1/Ang2 showed an apparent permeability of $(1.84 \pm 0.69) \times 10^{-7}$ and $(3.18 \pm 0.70) \times 10^{-7}$ cm s^{-1}, respectively. Moreover, transmission electron microscopy (TEM) images indicate that GNRs-Ang2 and GNRs-D1/Ang2 were released into the basal compartment (Fig. S2†), showing that both GNRs were transcytosed.

3.3 Brain delivery of GNRs-D1/Ang2 in a mouse transgenic model of AD

To evaluate the capacity of our GNRs-D1/Ang2 to reach the brains of AD transgenic mice (APPswe/PSEN1dE9), the AD mice were treated with a single i.v. dose of GNRs-D1/Ang2 (100 μL, 10 nM). After 15 minutes, the mice were anesthetized and subsequently perfused with PBS to remove blood. Brain and liver were removed, and gold content was quantified by neutron activation analysis; the percentage of the dose that reached these organs was calculated. Fig. 3 shows the percentage of the dose reaching the brain; for control GNRs-PEGs the percentage was 0.0157 ± 0.0151%, while for the GNRs-D1/Ang2 it was 0.043 ± 0.005%, significantly higher than the control. This result indicates that GNRs-D1/Ang2 reaches the brain

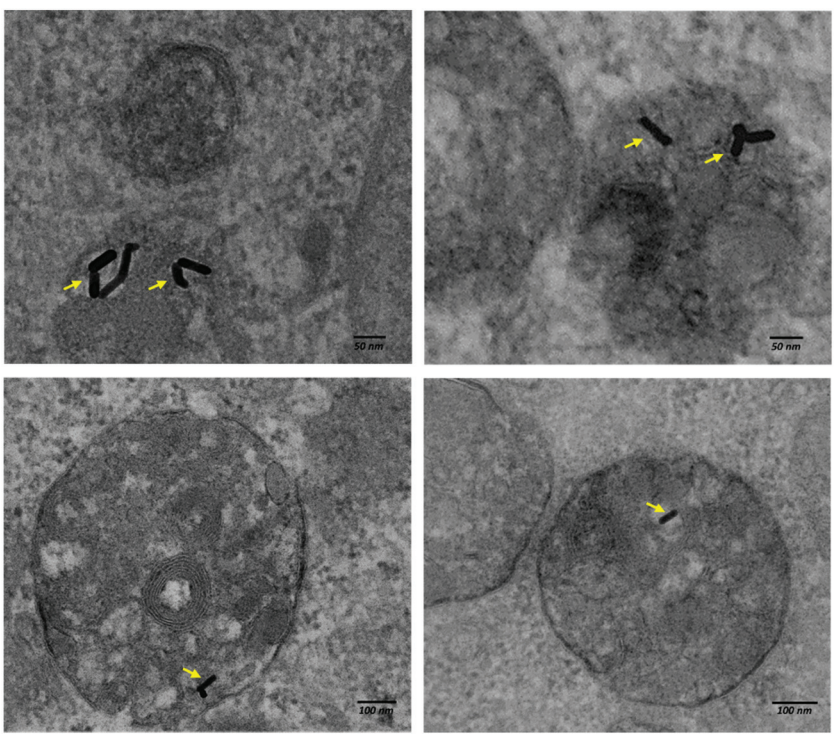

Fig. 2 Transmission electron microscopy (TEM) of bEnd.3 cells incubated with GNRs-D1/Ang2 [0.05 nM] for 24 hours. Yellow arrows indicate GNRs. Bar = 50 and 100 nm.

 This journal is © The Royal Society of Chemistry 2021

Published on 26 April 2021. Downloaded by University of Prince Edward Island on 5/16/2021 7:57:57 AM.

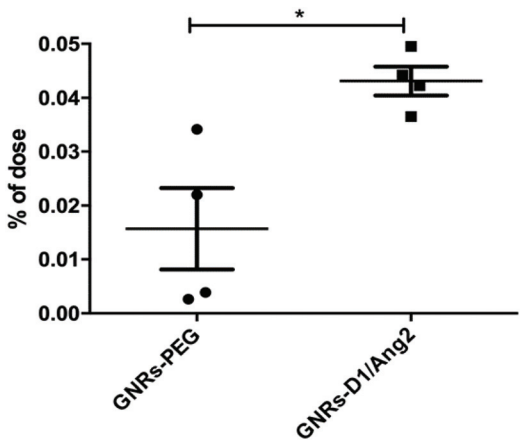

Fig. 3 Percentage of the gold dose that reached the brain. A total of 100 µl [10 nM] of GNRs-PEG or GNRs-D1/Ang2 were injected i.v. The animal was sacrificed at 15 minutes. Gold quantification was performed by neutron activation (CCHEN), $n = 4$. Mann–Whitney test, $p < 0.05$.

almost three times more than GNRs-PEGs, which agrees with the expected results according to our rationale design and the data by Velasco-Aguirre *et al.*, which described that the functionalization of GNRs with Ang2 improves the delivery of GNRs to the CNS, in comparison to GNRs-PEG alone in a healthy rat model.[12] Moreover, we confirmed the presence of GNRs-D1/Ang2 in the parenchyma of the hippocampus by STEM (Fig. 4). In order to determine whether GNRs-D1/Ang2 were localized in the amyloid plaques present in the brain, we also used a gold enhancement protocol with haematoxylin and Congo red staining (Fig. S3†). With this procedure, the nanoparticle acts as a nucleus for crystalline gold growth to form microparticles by reduction of gold catalyzed by the GNR, and can be visualized by optical microscopy.[54] Congo red allows detection of amyloid plaques.[55]

We also analysed the gold content in the liver and observed that there were no significant differences between the control GNRs-PEGs and GNRs-D1/Ang2, with retention values close to 30% of the dose for both groups, as shown in Fig. S5.† The accumulation of nanoparticles in organs related with the reticuloendotothelial system, such as the liver, spleen and kidney is expected. The accumulation of pegylated GNRs in these organs has been observed by other authors.[38,44] Future investigations will include a pharmacokinetic study to evaluate the accumulation and excretion of the nanoparticles, considering the potential theranostics application of the nanosystem.

Using Alexa Fluor 647-labeled GNRs as a control and GNRs-D1/Ang2, we then evaluated the localization of GNRs in brain slices of AD mice and their distribution with respect to amyloid plaques. The GNRs-D1/Ang2 labelled with Alexa Fluor 647 were administered intravenously. After 15 minutes, the mice were anesthetized, the brains were removed and fixed, and histological sections were acquired. The amyloid plaques were labelled by immunohistochemistry with WO2 antibodies

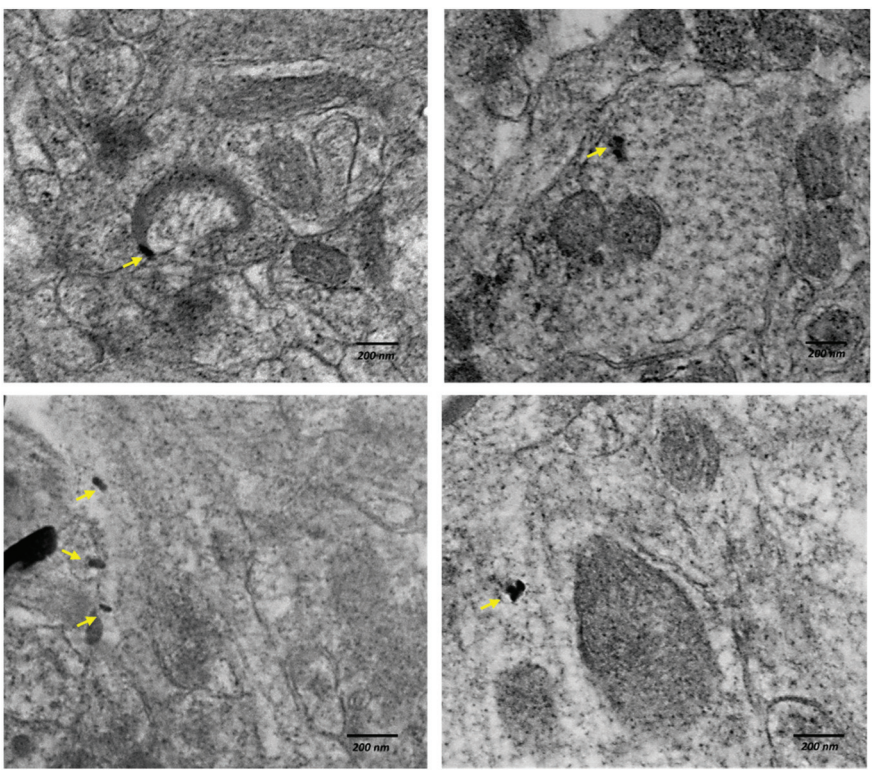

Fig. 4 STEM dark-field imaging of brain sections in hippocampal regions for the detection of GNRs-D1/Ang2. A total of 100 µl [10 nM] of GNRs-D1/Ang2 was injected i.v. Yellow arrows indicate the GNRs. Bar = 200 nm.

Published on 26 April 2021. Downloaded by University of Prince Edward Island on 5/16/2021 7:57:57 AM.

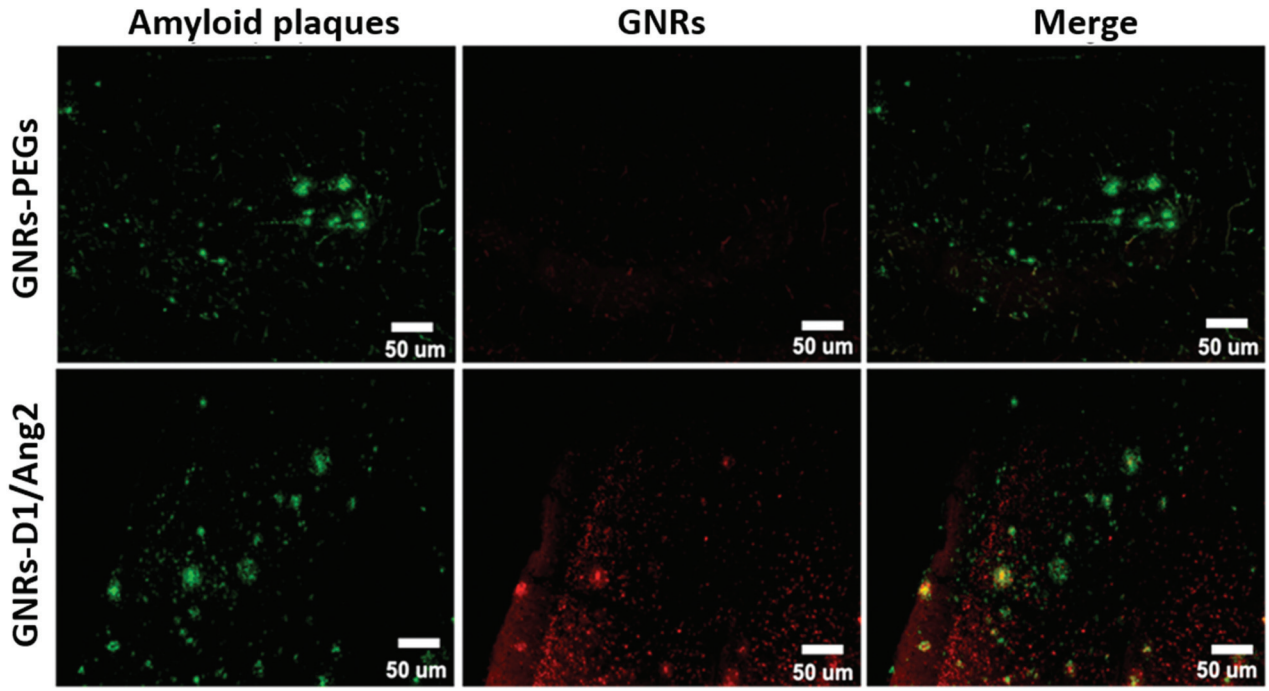

Fig. 5 Immunohistochemistry fluorescence imaging of brain slices from transgenic mouse models of Alzheimer's disease, after 15 min of the i.v. injection of 100 µl GNRs-D1/Ang2-Alexa Fluor 647 [10 nM]. The amyloid plaques are seen in green. The control was injected with GNRs-PEGs [10 nM].

and visualized in green (Alexa Fluor 488). We observed a clear Alexa Fluor 647 signal (red) in AD mice injected with GNRs-D1/Ang2-Alexa Fluor 647, which was concordant with the distribution of the WO2 green signal corresponding to amyloid plaques, while the AD mice injected with GNRs-PEGs-Alexa Fluor 647 showed a background red signal that was not coincident with amyloid plaques (Fig. 5). The overlapping signals were evaluated with the ImageJ-FIJI and Cell Profiler software, and the percentage of colocalization between the marks associated with GNRs-D1/Ang2 and the amyloid plaques was 22% (Fig. 6). For the GNRs-PEGs control, the percentage of overlapping signal was only 7%.

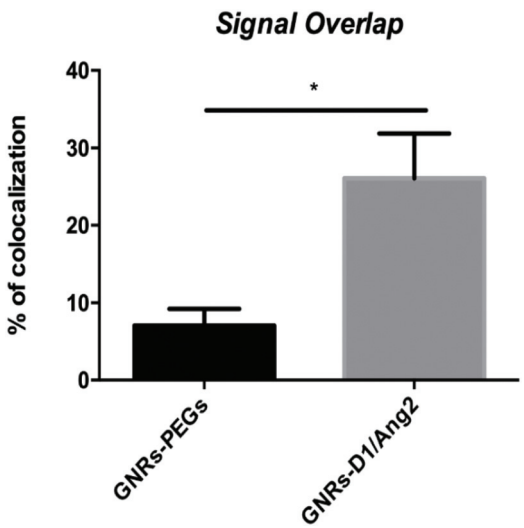

Fig. 6 Percentage of signal overlap of GNRs with the amyloid plaques from the *in vivo* experiment presented in Fig. 5. Mann–Whitney test, $p < 0.05$.

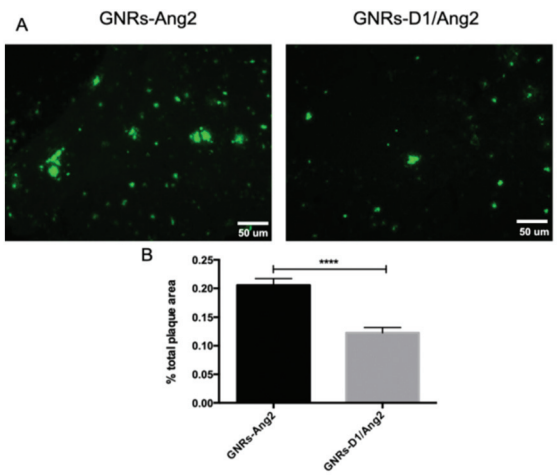

Fig. 7 Effects of GNRs-D1/Ang2 on amyloid load in the brain cortex. Animals treated with GNRs-D1/Ang2 (15 administrations in a 30 day period, 100 µL [10 nM], intraperitoneal, $n = 4$) showed a significant reduction of the amyloid load evaluated by thioflavin S, compared to the control group treated with GNRs-Ang2. (A) Representative image of cortex brain slices of animals treated with the GNRs-Ang2 and GNRs-D1/Ang2 nanosystems. (B) Quantification of the area occupied by amyloid plaques in the GNRs-Ang2 and GNRs-D1/Ang groups, expressed as a percentage of the occupied area with respect to the total image area. Mann–Whitney test, $p < 0.0001$.

 This journal is © The Royal Society of Chemistry 2021

Published on 26 April 2021. Downloaded by University of Prince Edward Island on 5/16/2021 7:57:57 AM.

3.4 Effect of recurrent treatment of AD mice with GNRs-D1/Ang2

Once we determined that our GNRs-D1/Ang2 nanosystem reached the CNS and located with the amyloid plaques, we evaluated whether GNRs-D1/Ang2 – where the D1 peptide recognizes and disaggregates amyloid aggregates – affected the amyloid load and inflammatory markers in AD mice. To this end, the AD mice were treated with GNRs-D1/Ang2 and GNRs-Ang2 as a control (100 μL, 10 nM) 15 times in a period of 30 days, after which the animals were anesthetized and perfused with PBS. The brains were extracted to evaluate the number of plaques and amyloid loads using thioflavin S, and GFAP was used to follow reactive astrocytes in the brain histological sections. The AD mice injected with GNRs-D1/Ang2 showed fewer and smaller amyloid plaques than those injected with control GNRs-Ang2 (Fig. 7A). Using the ImageJ and CellProfiler software, we quantified the number, the area and the intensity of the ThS signal associated with amyloid plaques and the percentage of plaque area with respect to total area in the GNRs-Ang2-treated control group and in the GNRs-D1/Ang2-treated group (Fig. 7B). In the experimental group, the percentage of the area occupied by the amyloid plaques in the cortex was lower than that of the control group. The GFAP signal for astrocytes was evaluated as a mark of brain inflammation and Fig. 8A shows that GFAP intensity was higher in the cortex of GNRs-Ang2-treated AD mice, compared to GNRs-D1/Ang2-treated AD mice. According to the quantification of the GFAP signal, lower levels of active astrocytes were found in the AD mice treated with GNRs-D1/Ang2 (Fig. 8B). These results agree with the design of our nanosystem as a theranostic tool. GNRs-D1/Ang2 were specifically targeted to amyloid plaques and served as a drug delivery device for D1, reducing the Aβ load. In this case, the control group treated with GNRs-Ang2 did not have the D1 therapeutic peptide, but the Ang2 peptide that improves delivery to the brain;[12] this group presented a higher number of amyloid plaques and a major area of the cortex occupied by the amyloid plaques, compared to the experimental group treated with GNRs-D1/Ang2. In the same way, the experimental group presented lower inflammation in the cortex, which correlated well with the decrease of the amyloid load in this region of the brain.

We can attribute the activity of a small quantity of nanoparticles that reach the brain to the local accumulation of the

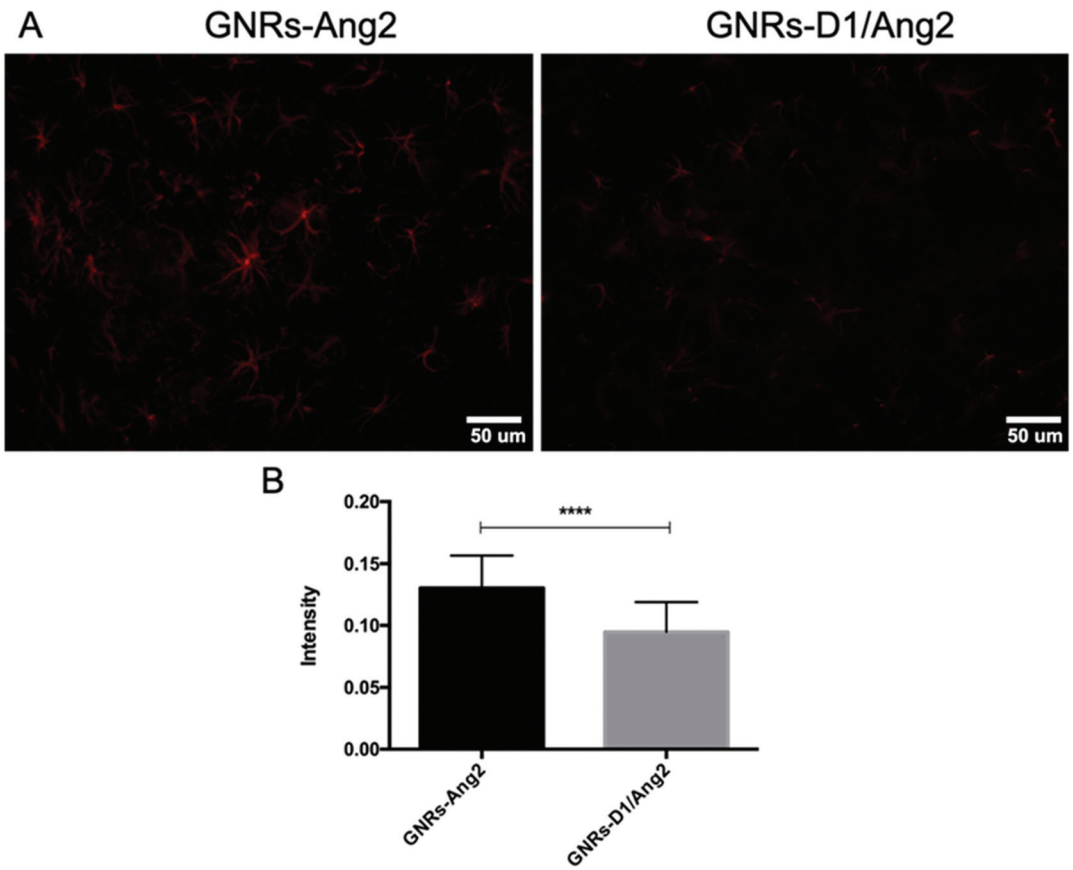

Fig. 8 Effect of GNRs-D1/Ang2 on GFAP intensity in the brain cortex. Animals treated with GNRs-D1/Ang2 (15 administrations in a 30 day period, 100 μL [10 nM], intraperitoneal, $n = 4$) showed a significant reduction of GFAP signal, as evaluated by immunofluorescence, compared to the control group treated with GNRs-Ang2. (A) Representative images of cortex brain slices of animals treated with the GNRs-Ang2 and GNRs-D1/Ang2 nanosystems. (B) Quantification of the GFAP signal intensity. Mann–Whitney test, $p < 0.0001$.

Published on 26 April 2021. Downloaded by University of Prince Edward Island on 5/16/2021 7:57:57 AM.

cargo (the D1 peptide) associated with the nanoparticle that produces an efficient effect. In another study, functionalized gold nanoparticles with glutathione, which exhibited similar levels of gold accumulation in the brain tissue after intravenous administration, allowed to rescue memory deficits in a mouse model of AD.[56] In order to increase the concentration of nanoparticles in the brain, we considered intranasal administration, which is very efficient to deliver gold nanoparticles functionalized with the peptide D1, as we showed recently.[57]

Importantly, after the chronic treatment, the animals did not show significant indicatives of distress, toxicity, pain or discomfort, such as irregular respiration, loss of hair, ataxia or other motor disabilities, nor death. However, considering potential theranostic applications of the nanosystem, a complete biodistribution and toxicity profile will be performed in future studies.

3.5 *In vivo* detection of GNRs-D1/Ang2 by micro-CT

Taking advantage of the high X-ray attenuation coefficient of gold,[6,10,33] we determined by the micro-CT technique the presence of GNRs in the CNS *in vivo*, considering the possibility of applying our nanosystem as an *in vivo* diagnostic method for AD.

Before being sacrificed, the AD mice treated with GNRs-Ang2 and GNRs-D1/Ang2 through 15 injections over 30 days were analyzed by micro-CT. The micro-CT signals were higher in animals treated with GNRs-D1/Ang2 than in those treated with GNRs-Ang2, as shown in Fig. 9 (ESI Movies S1 and S2,† respectively). In Fig. 9, A and C correspond to the animal treated with GNRs-Ang2, in the sagittal and frontal sections, respectively. The signal associated with the GNRs was located only in the center of the brain, in a straight line that crossed the brain, which could be attributed to the nanoparticles present in the circulation. On the other hand, in the animals treated with GNRs-D1/Ang2 (Fig. 9B and D), the signals associated with the GNRs were observed in different brain regions, which are related to the accumulation of amyloid plaques in this model *in vivo*.[58] This difference supports the notion that the presence of the D1 peptide in the nanosystem allows its retention in the brain of AD mice. This result is in agreement with the rationale design of our nanosystem, as the D1 peptide is essential for the capacity to recognize the Aβ aggregates present in the brain with AD.

Finally, to determine whether a single dose of the nanosystem allowed the detection of the presence of GNRs-D1/Ang2 associated with amyloid aggregates in the brain, we evaluated differences in the GNR signal between healthy and AD animals. We performed micro-CT scans of the TG and WT animals that were treated with GNRs-D1/Ang2 for 15 minutes to assess whether the presence of GNRs in the brain of our AD animal model could be detected with a single dose and if there were differences in this signal, compared with healthy animals. As shown in Fig. 10, we detected a higher signal associated with GNRs in the brain of AD animals compared to the signal in the WT animals (ESI Movies S3 and S4,† respectively). Furthermore, we observed a high signal in the cerebellum of the TG animal. According to Ordoñez-Gutierrez *et al.*, 2016, β-amyloid aggregates in the cerebellum of this transgenic

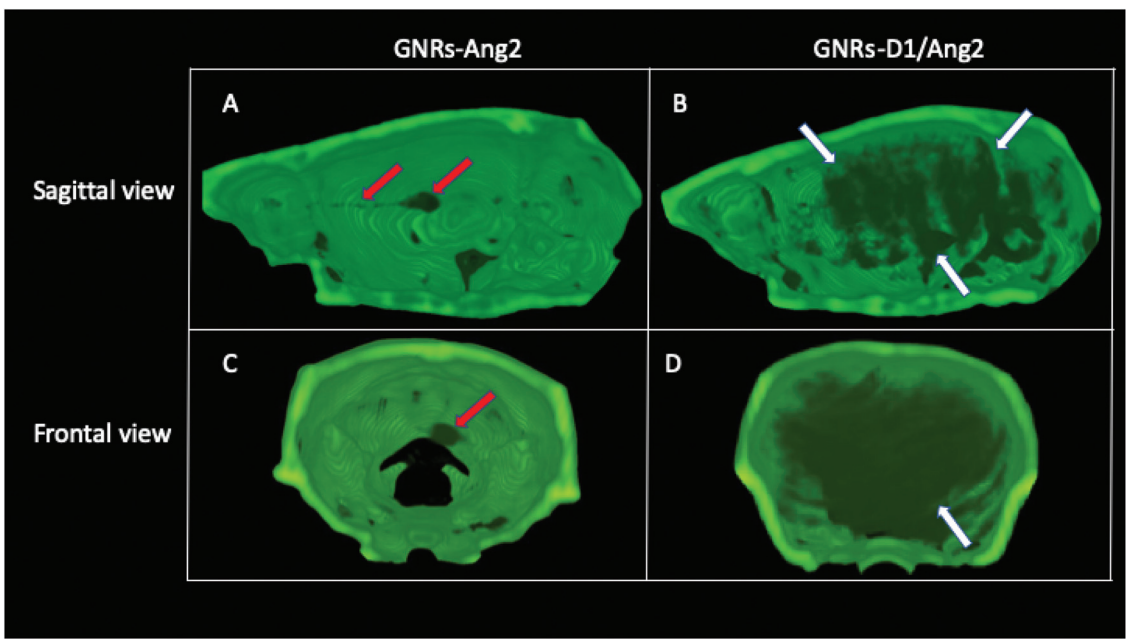

Fig. 9 Images of the skull by micro-CT of transgenic APPswe/PSEN1dE9 mice treated for one month (15 administrations) with 100 μL of GNRs-D1/Ang2 or GNRs-Ang2 10 nM. (A) Sagittal section of a transgenic mouse treated with GNRs-Ang2. (B) Sagittal section of a transgenic mouse treated with GNRs-D1/Ang2. (C) Frontal section of a transgenic mouse treated with GNRs-Ang2. (D) Frontal section of a transgenic mouse treated with GNRs-D1/Ang2. The white arrows indicate accumulation of gold nanoparticles in the amyloid aggregates. The red arrows indicate accumulation of gold nanoparticles in the circulation.

 This journal is © The Royal Society of Chemistry 2021

Published on 26 April 2021. Downloaded by University of Prince Edward Island on 5/16/2021 7:57:57 AM.

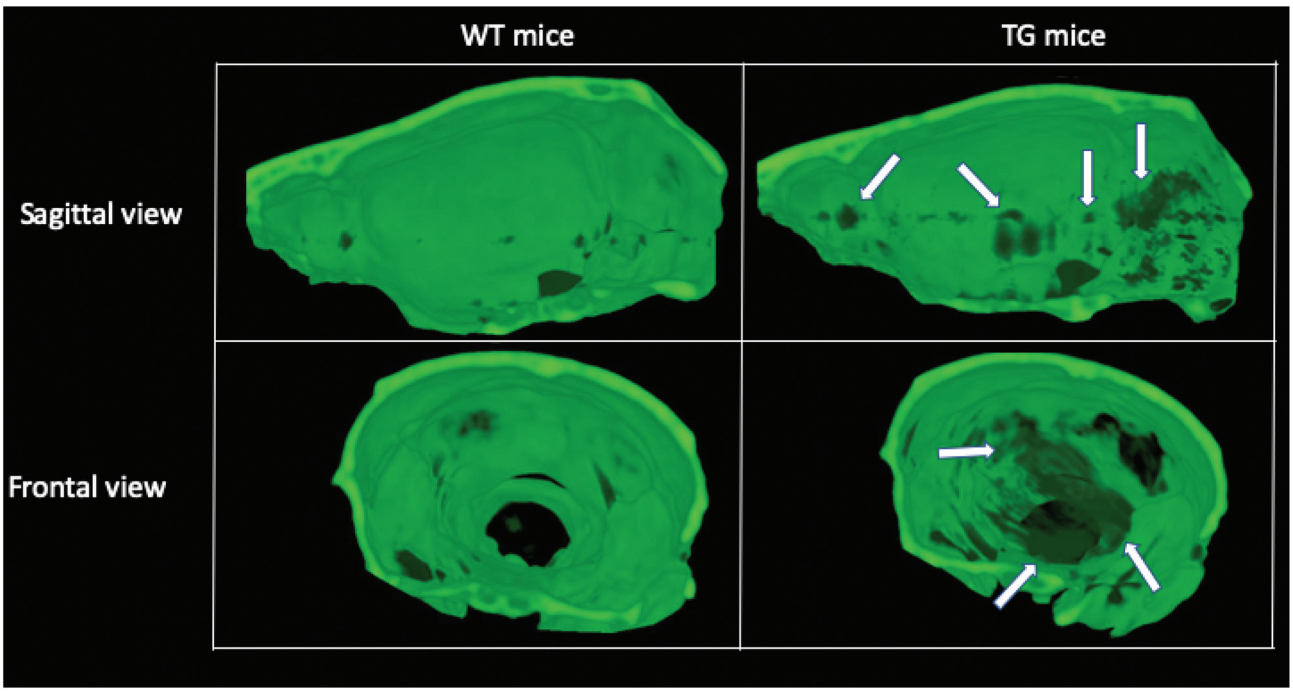

Fig. 10 Animals treated with a single dose of GNRs-D1/Ang2 (10 nM). Images of the skull by micro-CT of transgenic APPswe/PSEN1dE9 mice (TG) or wild type C57BL/6 mice (WT, healthy) treated with an i.v. single dose of 100 μL of GNRs-D1/Ang2. Sagittal sections (upper panels) and frontal sections (lower panels) of mice treated with GNRs-D1/Ang2 are shown. The white arrows indicate the signal associated with the presence of GNRs.

mouse AD model,[58] and therefore our results support the early interaction of the circulating GNRs with Aβ deposits.

In the case of animals treated with GNRs-PEG (Fig. S6 and ESI Movie S5†), only one signal associated with GNRs was detected in the center of the brain, forming a straight line through it, very similar to that observed in control animals treated with GNRs-Ang2 for 30 days, which could be related to the GNRs in circulation. For WT C57BL/6 animals treated with a single dose of GNRs-PEG or without treatment (Fig. S7 and S8†), we did not detect signals associated with the presence of GNRs in the brain.

4. Conclusions

To the best of knowledge, we have developed for the first time an *in vivo* therapeutic peptide delivery system based on GNRs, with theranostic potential for application in AD, and compatible with the micro-CT methodology. The GNRs functionalized with the Ang2 and D1 peptides induced the diminution of both the amyloid load and inflammatory markers in the brain of our murine AD model by using a micro-CT. Moreover, we observed differences in the *in vivo* detection of GNRs-D1/Ang2 between WT and AD mice, when we analyzed both the brain of the animals treated for one month and those treated with a single-dose of the nanosystem. We demonstrated that the multi-functionalization of the GNRs with two peptides (Ang2 and D1) improved the delivery and retention of this nanosystem in the brain, reinforcing the therapeutic benefits associated with the β sheet breaker ability of the D1 peptide. Based on our results, the GNRs-D1/Ang2 nanosystem could be useful as a theranostic system for AD. Notably, other routes to improve the delivery of nanoparticles to the brain should be explored, such as intranasal administration. In relation with these experiments *in vivo* studies are currently in progress in our laboratory.

Ethical statement

All animal procedures were performed in accordance with the Guidelines for Care and Use of Laboratory Animals of the University of Chile and approved by the Animal Ethics Committee of this University.

Conflicts of interest

Figures of this paper were created with the aid of BioRender. The authors report no conflicts of interest, financial or otherwise, in this research.

Acknowledgements

We thank the Plataforma Experimental Bio-CT, Faculty of Dentistry from Universidad de Chile (FONDEQUIP EQM150010) for performing the Micro-CT analysis and Fondequip EQM170111, and the Fondecyt 1170929, 1211482,

Published on 26 April 2021. Downloaded by University of Prince Edward Island on 5/16/2021 7:57:57 AM.

1190623, 1201668, Fondap 15130011, Beca Doctorado 21180739, and Fondecyt 3190547 grants. Peptide synthesis D1 was performed at the NANBIOSIS–CIBER BBN Peptide Synthesis Unit (U3).

Notes and references

1 D. Cabuzu, A. Cirja, R. Puiu and A. M. Grumezescu, *Curr. Top. Med. Chem.*, 2015, **15**, 1605–1613.
2 S. Link and M. A. El-Sayed, *Annu. Rev. Phys. Chem.*, 2003, **54**, 331–366.
3 C. Adura, S. Guerrero, E. Salas, L. Medel, A. Riveros, J. Mena, J. Arbiol, F. Albericio, E. Giralt and M. J. Kogan, *ACS Appl. Mater. Interfaces*, 2013, **5**, 4076–4085.
4 C. Velasco-Aguirre, F. Morales, E. Gallardo-Toledo, S. Guerrero, E. Giralt, E. Araya and M. J. Kogan, *Int. J. Nanomed.*, 2015, **10**, 4919–4936.
5 X. Han, K. Xu, O. Taratula and K. Farsad, *Nanoscale*, 2019, **11**, 799–819.
6 O. Betzer, N. Perets, A. Angel, M. Motiei, T. Sadan, G. Yadid, D. Offen and R. Popovtzer, *ACS Nano*, 2017, **11**, 10883–10893.
7 Y. H. Liao, Y. J. Chang, Y. Yoshiike, Y. C. Chang and Y. R. Chen, *Small*, 2012, **8**, 3631–3639.
8 A. Del Sole, *Funct. Neurol.*, 2016, **31**, 205–215.
9 M. M. Svedberg, O. Rahman and H. Hall, *Nucl. Med. Biol.*, 2012, **39**, 484–501.
10 P. H. Kee and D. Danila, *Nanomedicine*, 2018, **14**, 1941–1947.
11 F. Morales-Zavala, H. Arriagada, N. Hassan, C. Velasco, A. Riveros, A. R. Álvarez, A. N. Minniti, X. Rojas-Silva, L. L. Muñoz, R. Vasquez, K. Rodriguez, M. Sanchez-Navarro, E. Giralt, E. Araya, R. Aldunate and M. J. Kogan, *Nanomedicine*, 2017, **13**, 2341–2350.
12 C. Velasco-Aguirre, F. Morales-Zavala, E. Salas-Huenuleo, E. Gallardo-Toledo, O. Andonie, L. Munoz, X. Rojas, G. Acosta, M. Sanchez-Navarro, E. Giralt, E. Araya, F. Albericio and M. J. Kogan, *Nanomedicine*, 2017, **12**, 2503–2517.
13 P. H. Yang, X. Sun, J. F. Chiu, H. Sun and Q. Y. He, *Bioconjug. Chem.*, 2005, **16**, 494–496.
14 A. R. Rastinehad, H. Anastos, E. Wajswol, J. S. Winoker, J. P. Sfakianos, S. K. Doppalapudi, M. R. Carrick, C. J. Knauer, B. Taouli, S. C. Lewis, A. K. Tewari, J. A. Schwartz, S. E. Canfield, A. K. George, J. L. West and N. J. Halas, *Proc. Natl. Acad. Sci. U. S. A.*, 2019, **116**, 18590–18596.
15 S. Nardecchia, P. Sánchez-Moreno, J. d. Vicente, J. A. Marchal and H. Boulaiz, *Nanomaterials*, 2019, **9**, 191.
16 A. N. Kharlamov, J. A. Feinstein, J. A. Cramer, J. A. Boothroyd, E. V. Shishkina and V. Shur, *Future Cardiol.*, 2017, **13**, 345–3363.
17 G. E. Abraham and P. B. Himmel, *J. Nutr. Environ. Med.*, 1997, **7**, 295–305.
18 S. K. Libutti, G. F. Paciotti, A. A. Byrnes, H. R. Alexander, W. E. Gannon, M. Walker, G. D. Seidel, N. Yuldasheva and L. Tamarkin, *Clin. Cancer Res.*, 2010, **16**, 6139–6149.
19 M. Khoobchandani, K. K. Katti, A. R. Karikachery, V. C. Thipe, D. Srisrimal, D. K. Dhurvas Mohandoss, R. D. Darshakumar, C. M. Joshi and K. V. Katti, *Journal*, 2020, **15**, 181–197.
20 M. R. K. Ali, Y. Wu and M. A. El-Sayed, *J. Phys. Chem. C*, 2019, **123**, 15375–15393.
21 H. A.-O. Arami, C. B. Patel, S. A.-O. Madsen, P. J. Dickinson, R. A.-O. Davis, Y. Zeng, B. K. Sturges, K. D. Woolard, F. G. Habte, D. Akin, R. Sinclair and S. A.-O. Gambhir, *ACS Nano*, 2019, **13**, 2858–2869.
22 P. Jara-Guajardo, P. Cabrera, F. Celis, M. Soler, I. Berlanga, N. Parra-Muñoz, G. Acosta, F. Albericio, F. Guzman, M. Campos, A. Alvarez, F. Morales-Zavala and M. J. Kogan, *Nanomaterials*, 2020, **10**, 690.
23 E. Karran, M. Mercken and B. De Strooper, *Nat. Rev. Drug Discovery*, 2011, **10**, 698–712.
24 C. Ballard, S. Gauthier, A. Corbett, C. Brayne, D. Aarsland and E. Jones, *Lancet*, 2011, **377**, 1019–1031.
25 W. L. Klein, *J. Alzheimers Dis.*, 2013, **33**(Suppl 1), S49–S65.
26 P. N. Lacor, M. C. Buniel, L. Chang, S. J. Fernandez, Y. Gong, K. L. Viola, M. P. Lambert, P. T. Velasco, E. H. Bigio, C. E. Finch, G. A. Krafft and W. L. Klein, *J. Neurosci.*, 2004, **24**, 10191–10200.
27 W. Q. Zhao, F. G. De Felice, S. Fernandez, H. Chen, M. P. Lambert, M. J. Quon, G. A. Krafft and W. L. Klein, *FASEB J.*, 2008, **22**, 246–260.
28 E. Araya, I. Olmedo, N. G. Bastus, S. Guerrero, V. F. Puntes, E. Giralt and M. J. Kogan, *Nanoscale Res. Lett.*, 2008, **3**, 435–443.
29 S. Guerrero, E. Araya, J. L. Fiedler, J. I. Arias, C. Adura, F. Albericio, E. Giralt, J. L. Arias, M. S. Fernández and M. J. Kogan, *Nanomedicine*, 2010, **5**, 897–913.
30 S. A. Funke, D. Bartnik, J. M. Glück, K. Piorkowska, K. Wiesehan, U. Weber, B. Gulyas, C. Halldin, A. Pfeifer, C. Spenger, A. Muhs and D. Willbold, *PLoS One*, 2012, **7**, e41457.
31 K. Wiesehan, J. Stöhr, L. Nagel-Steger, T. van Groen, D. Riesner and D. Willbold, *Protein Eng. Des. Sel.*, 2008, **21**, 241–246.
32 D. Xue, M. Zhao, Y.-j. Wang, L. Wang, Y. Yang, S.-w. Wang, R. Zhang, Y. Zhao and R.-t. Liu, *Neurobiol. Dis.*, 2012, **46**, 701–709.
33 N. Perets, O. Betzer, R. Shapira, S. Brenstein, A. Angel, T. Sadan, U. Ashery, R. Popovtzer and D. Offen, *Nano Lett.*, 2019, **19**, 3422–3431.
34 B. Nikoobakht and M. A. El-Sayed, *Chem. Mater.*, 2003, **15**, 1957–1962.
35 X. Huang, X. Peng, Y. Wang, Y. Wang, D. M. Shin, M. A. El-Sayed and S. Nie, *ACS Nano*, 2010, **4**, 5887–5896.
36 A. Tapia-Arellano, E. Gallardo-Toledo, C. Ortiz, J. Henríquez, C. G. Feijóo, E. Araya, R. Sierpe and M. J. Kogan, *Mater. Sci. Eng., C*, 2021, **121**, 111785.
37 J.-L. Wang, X.-J. Du, J.-X. Yang, S. Shen, H.-J. Li, Y.-L. Luo, S. Iqbal, C.-F. Xu, X.-D. Ye, J. Cao and J. Wang, *Biomaterials*, 2018, **182**, 104–113.

 This journal is © The Royal Society of Chemistry 2021

Published on 26 April 2021. Downloaded by University of Prince Edward Island on 5/16/2021 7:57:57 AM.

38 D. P. K. Lankveld, R. G. Rayavarapu, P. Krystek, A. G. Oomen, H. W. Verharen, T. G. van Leeuwen, W. H. De Jong and S. Manohar, *Nanomedicine*, 2011, **6**, 339–349.
39 L. Li, J. Cui, Z. Liu, X. Zhou, Z. Li, Y. Yu, Y. Jia, D. Zuo and Y. Wu, *Toxicol. Lett.*, 2018, **285**, 156–167.
40 M. Das, D. K. Yi and S. S. An, *Int. J. Nanomed.*, 2015, **20**(10), 1521–1545.
41 Y. Xiao, E. Zhang and A. Fu, *Nanoscale Res. Lett.*, 2017, **12**, 641.
42 R. Chakraborty, D. Leshem-Lev, R. Kornowski and D. Fixler, *Nano Lett.*, 2020, **20**, 8360–8368.
43 H. Jiang, D. Chen, D. Guo, N. Wang, Y. Su, X. Jin, G. Tong and X. Zhu, *Biomater. Sci.*, 2017, **5**, 686–697.
44 G. Alfranca, L. Beola, Y. Liu, L. Gutiérrez, A. Zhang, A. Artiga, D. Cui and J. M. de la Fuente, *Nanomedicine*, 2019, **14**, 3035–3055.
45 L. D. Estrada, D. Chamorro, M. J. Yanez, M. Gonzalez, N. Leal, R. von Bernhardi, A. E. Dulcey, J. Marugan, M. Ferrer, C. Soto, S. Zanlungo, N. C. Inestrosa and A. R. Alvarez, *J. Alzheimers Dis.*, 2016, **54**, 1193–1205.
46 M. A. Chacón, M. I. Barría, C. Soto and N. C. Inestrosa, *Mol. Psychiatry*, 2004, **9**, 953–961.
47 A. Subtil, A. Hemar, A. Fau-Dautry-Varsat and A. Dautry-Varsat, *J. Cell Sci.*, 1994, **107**, 3461–3468.
48 M. Demeule, J.-C. Currie, Y. Bertrand, C. Ché, T. Nguyen, A. Régina, R. Gabathuler, J.-P. Castaigne and R. Béliveau, *J. Neurochem.*, 2008, **106**(4), 1534–1544.
49 B. Yameen, W. I. Choi, C. Vilos, A. Swami, J. Shi and O. C. Farokhzad, *J. Control. Release*, 2014, **190**, 485–499.
50 R. Cecchelli, S. Aday, E. Sevin, C. Almeida, M. Culot, L. Dehouck, C. Coisne, B. Engelhardt, M.-P. Dehouck and L. Ferreira, *PLoS One*, 2014, **9**, e99733.
51 B. Oller-Salvia, M. Sánchez-Navarro, S. Ciudad, M. Guiu, P. Arranz-Gibert, C. Garcia, R. R. Gomis, R. Cecchelli, J. García, E. Giralt and M. Teixidó, *Angew. Chem., Int. Ed.*, 2016, **55**, 572–575.
52 T.-G. Zhan, H.-H. Yin, S.-T. Zheng, W.-C. Lin, N.-L. Shen, J. Cui, L.-C. Kong, L.-J. Liu and K.-D. Zhang, *Chem. Commun.*, 2018, **54**, 9356–9359.
53 D. Ye, M. N. Raghnaill, M. Bramini, E. Mahon, C. Åberg, A. Salvati and K. A. Dawson, *Nanoscale*, 2013, **5**, 11153–11165.
54 S. Guerrero, V. M. Díaz-García, P. Contreras-Orellana, P. Lara, S. Palma, F. Guzman, L. Lobos-Gonzalez, A. Cárdenas, X. Rojas-Silva, L. Muñoz, L. Leyton, M. J. Kogan and A. F. G. Quest, *Nanomedicine*, 2018, **13**, 1447–1462.
55 H. B. Rajamohamedsait and E. M. Sigurdsson, *Methods Mol. Biol.*, 2012, **849**, 411–424.
56 K. Hou, J. Zhao, H. Wang, B. Li, K. Li, X. Shi, K. Wan, J. Ai, J. Lv, D. Wang, Q. Huang, H. Wang, Q. Cao, S. Liu and Z. Tang, *Nat. Commun.*, 2020, **11**, 4790.
57 E. Gallardo-Toledo, A. Tapia-Arellano, F. Celis, T. Sinai, M. Campos, M. J. Kogan and A. C. Sintov, *Int. J. Pharm.*, 2020, **590**, 119957.
58 L. Ordoñez-Gutierrez, I. Fernandez-Perez, J. L. Herrera, M. Anton, I. Benito-Cuesta and F. Wandosell, *J. Alzheimer's Dis.*, 2016, **54**, 645–656.